Critical impact of vegetation physiology on the continental hydrologic cycle in response to increasing CO_2

Léo Lemordant[a,1], Pierre Gentine[a,b,1], Abigail S. Swann[c,d], Benjamin I. Cook[e,f], and Jacob Scheff[g]

[a]Earth and Environmental Engineering Department, Columbia University, New York, NY 10027; [b]Earth Institute, Columbia University, New York, NY 10025; [c]Department of Atmospheric Sciences, University of Washington, Seattle, WA 98105; [d]Department of Biology, University of Washington, Seattle, WA 98195; [e]NASA Goddard Institute for Space Studies, New York, NY 10025; [f]Ocean and Climate Physics, Lamont-Doherty Earth Observatory, Palisades, NY 10964; and [g]Department of Geography & Earth Sciences, University of North Carolina at Charlotte, Charlotte, NC 28223

Predicting how increasing atmospheric CO_2 will affect the hydrologic cycle is of utmost importance for a range of applications ranging from ecological services to human life and activities. A typical perspective is that hydrologic change is driven by precipitation and radiation changes due to climate change, and that the land surface will adjust. Using Earth system models with decoupled surface (vegetation physiology) and atmospheric (radiative) CO_2 responses, we here show that the CO_2 physiological response has a dominant role in evapotranspiration and evaporative fraction changes and has a major effect on long-term runoff compared with radiative or precipitation changes due to increased atmospheric CO_2. This major effect is true for most hydrological stress variables over the largest fraction of the globe, except for soil moisture, which exhibits a more nonlinear response. This highlights the key role of vegetation in controlling future terrestrial hydrologic response and emphasizes that the carbon and water cycles are intimately coupled over land.

water cycle | vegetation physiology | climate change | land–atmosphere coupling | hydrology

Most of our understanding of changes in water availability is based on the analysis of changes in the imbalance between precipitation (P) and total evaporation (E) (1, 2). Over open water bodies, evaporation is at its potential rate, i.e., potential evaporation E_p (3, 4). However, over land, soil and vegetation limit the supply of moisture to the atmosphere so that the actual evapotranspiration (ET) is lower than the atmospheric demand E_p. Hence on vegetated surfaces, the analysis of $P − E_p$ fails to explain the projected changes in actual water fluxes (5–7), or even the direction of the change in many regions of the globe, and in particular in the subtropics (5, 8, 9). The supply of ET is controlled by the transport of water from the soil and plant roots to the atmosphere and thus depends on moisture available in the soil, biomass (particularly leaf area), plant hydraulic stress, and the opening of stomata (small pores at the leaf surface) among other things. The atmospheric demand of ET is driven by the temperature and dryness of the air, wind speed, and available radiation (as given by the Penman–Monteith equation). As a result, ET and P-ET over land can substantially differ from their potential rates E_p, and $P − E_p$, respectively (6, 7, 10).

Plant transpiration accounts for the largest fraction of terrestrial ET (11), and rising atmospheric $[CO_2]$ affects transpiration through the regulation of stomata (12). With increasing $[CO_2]$ at the leaf surface, the density of stomata at the leaf surface is decreased and their individual opening is reduced and therefore less water is transpired per unit leaf area (13, 14). In other words, leaf-level water use efficiency increases (12, 15, 16), potentially increasing surface soil moisture (17, 18) and runoff (19). On the other hand, leaf biomass tends to also increase with increasing $[CO_2]$, as reported in several field experiments (12, 15, 16, 20), generating a larger evaporative surface that can partly offset the reduction in stomatal conductance and negate the soil water savings (17). Our objective is therefore to quantify how such plant $[CO_2]$ effects influence future hydrological variable responses compared with radiative effects

(21)—the atmospheric impact of the "greenhouse effect." Radiative effects impact precipitation, i.e., water supply, and evaporative demand, through increase in radiation, temperature, and atmospheric dryness as estimated by the vapor pressure deficit (VPD), i.e., saturation minus actual vapor pressure (Fig. 1).

Results

Several dryness indices based on E_p have been previously defined and used to assess changes in water stress, but give contradictory responses (22–24). We therefore decided to not use such indices [e.g., Swann et al. (6)] as they are not pertinent in the future because of plant physiological effects [Swann et al. (6) and Milly and Dunne (7)]. We instead focus on actual physical variables that can be used as land aridity indicators pertinent to various applications. P-ET is a good proxy for long-term runoff, as soil and groundwater storage variations over several years are negligible, and a useful variable for agricultural and ecological impacts. In addition to P-ET, we focus on three variables (Fig. 2): soil moisture (agronomy and ecology), ET (hydrology, climate), and evaporative fraction (EF) (land–atmosphere interactions), i.e., the ratio of ET to surface available energy.

Disentangling Atmospheric and Physiological Responses to Increasing CO_2. We quantify changes in these water cycle parameters using a multimodel ensemble from Phase 5 of the Coupled Model

---

Significance

Predicting how increasing atmospheric CO_2 will affect the hydrologic cycle is of utmost importance for a wide range of applications. It is typically thought that future dryness will depend on precipitation changes, i.e., change in water supply, and changes in evaporative demand due to either increased radiation or temperature. Opposite to this viewpoint, using Earth system models, we show that changes in key water-stress variables will be strongly modified by vegetation physiological effects in response to increased $[CO_2]$ at the leaf level. These results emphasize that the continental carbon and water cycles have to be studied as an interconnected system.
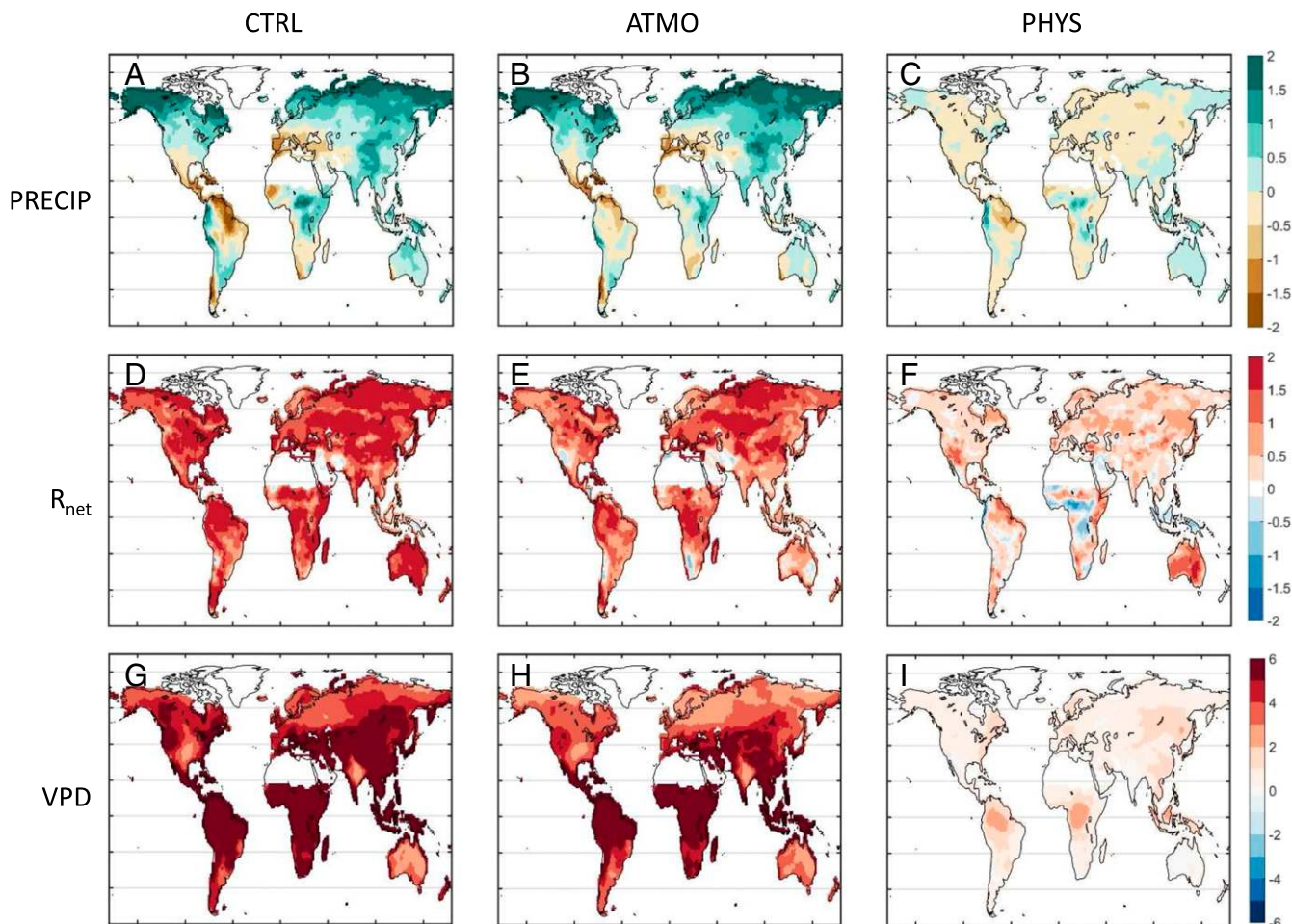
EARTH, ATMOSPHERIC, AND PLANETARY SCIENCES

Fig. 1. Supply and demand for water. Precipitation (*A–C*; annual) is the supply; demand for water is driven by two factors: net radiation (*D–F*; annual) and VPD (*G–I*; growing season) for, respectively, CTRL (*Left*), ATMO (*Center*), and PHYS (*Right*) runs. Change is quantified by the difference of the years 89–118 of the simulation and the years 1–20, normalized by the SD of CTRL over the years 1–20 (*Materials and Methods*). The changes observed for VPD are much larger in amplitude than for R_n and P, so that the scale was adjusted accordingly for VPD in *G*.

Intercomparison Project CMIP5 (25), and assess the impact of atmospheric (ATMO) vs. physiological (PHYS) CO_2 effects (21) using an idealized experiment where $[CO_2]$ is increased from preindustrial levels by 1% each year only in the atmospheric model (ATMO) or in the vegetation model (PHYS), or in both (CTRL) (*Materials and Methods*). These conceptual experiments give geographically consistent results with the more commonly used Representative Concentration Pathways 8.5 (RCP 8.5) experiments (*SI Appendix*, Figs. S1–S3), and enable us to disentangle the greenhouse gas warming (ATMO) from the physiological effects of increased $[CO_2]$ (PHYS) on hydrologic responses. We further decompose the global warming effects in ATMO into the contribution of precipitation and net radiation (and related increases in temperature and VPD) (*Materials and Methods*). We are then able to estimate the relative contribution of each of the three main hydrologic drivers: precipitation, net radiation, and physiological effects (Fig. 3 and *SI Appendix*, Fig. S4), as well as nonlinearities that could result from the interactions between surface physiology and atmospheric changes (*Materials and Methods*).

The drivers of water supply and evaporative demand—precipitation, radiation, and VPD—are primarily controlled by atmospheric greenhouse effects (ATMO) (Fig. 1). On the supply side of the water balance, annual precipitation increases throughout the globe in CTRL, because of the increased energy input into the surface due to increased greenhouse gas effects and because of the increased atmospheric water vapor, especially at northern latitudes (Fig. 1*A*) where the present pattern is exacerbated by

warming-induced changes in water vapor (1, 26, 27). Precipitation decreases in several places such as in Southwest North America, southern Africa, the Amazon, and the Mediterranean region (2), primarily because of global warming (Fig. 1*B*) and changes in atmospheric dynamics and not because of physiological effects, which mainly have an impact on tropical precipitation (Fig. 1*C*).

On the demand side of the water balance, net radiation (R_n), one of the main drivers of E_p (3), increases relatively uniformly over the Earth (Fig. 1*D*) in CTRL, primarily driven by greenhouse gas radiative effects (Fig. 1*E*). Nonetheless, physiological effects also increase R_n throughout the globe except in equatorial Africa and in Indonesia (Fig. 1*F*). The reduction in low cloud cover imposed by the decreased EF (28) (Fig. 2*I*) drives a downwelling shortwave radiation increase, while the limited differential changes in surface skin and air temperature keep longwave radiation changes small.

Enhanced VPD not only increases evaporative demand [Penman's equation (3)] but also decreases stomatal conductance, and therefore ET. VPD increases strongly across the Earth with increasing $[CO_2]$ (Fig. 1*G*) due to its exponential dependence on temperature (Fig. 1*H* and *SI Appendix*, Fig. S5). In addition to warming effects (Fig. 1*H*), the closure of stomata under higher $[CO_2]$ implies reduced water flux into the air. The resulting shift in EF (Fig. 2*I*) contributes to higher temperatures, which, combined with lower humidity, increases VPD throughout the globe, especially in the wet tropics (Fig. 1*I*). Climate change also drives
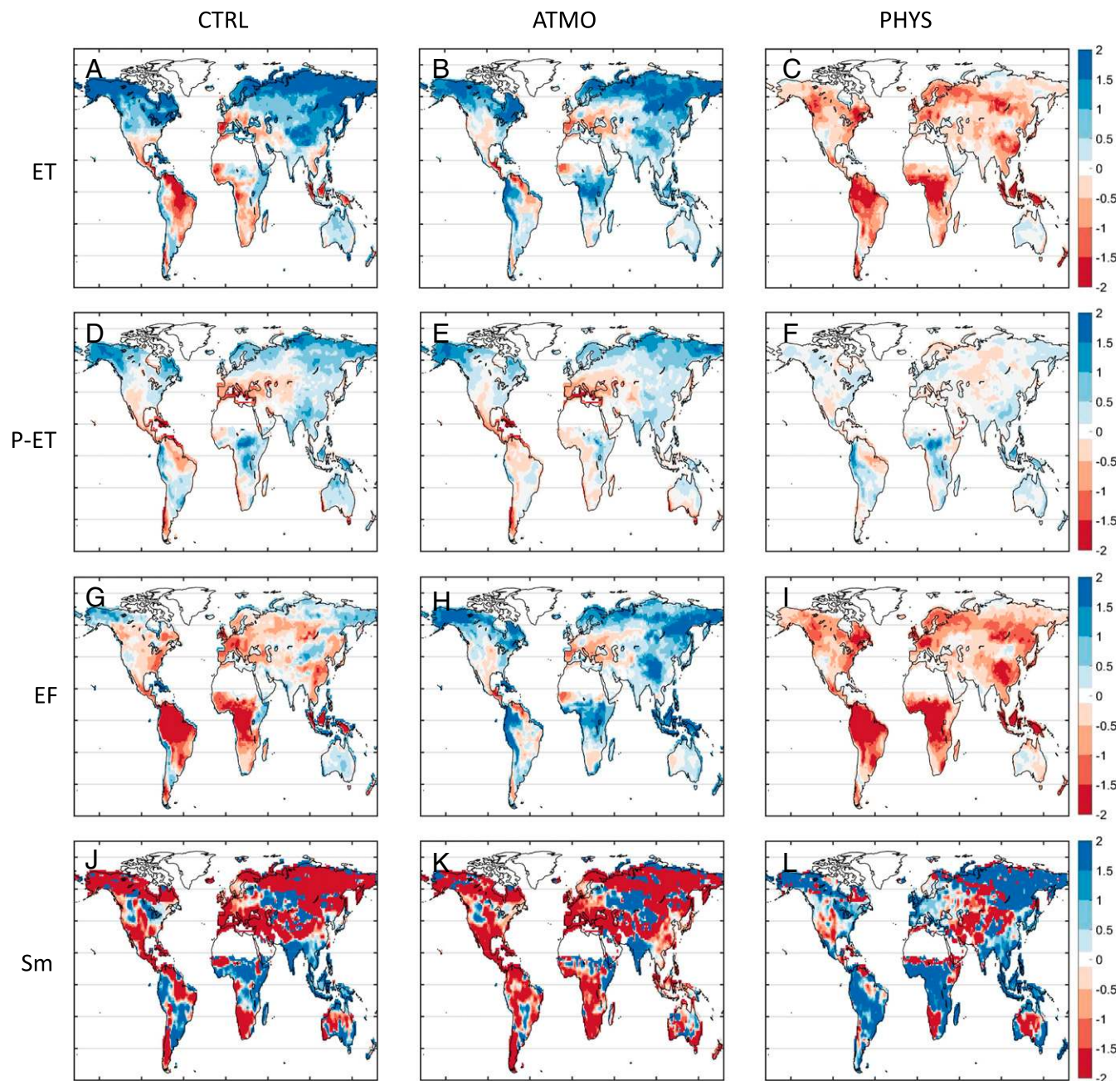
Fig. 2. Hydrologic cycle response to increased [CO_2]. ET (*A–C*; annual), P-ET (*D–F*; annual), EF (*G–I*; growing season), soil moisture at 2 m (*J–L*; growing season), changes in CTRL (*Left*), ATMO (*Center*), and PHYS (*Right*) runs are quantified by the difference of the years 89–118 of the simulation and the years 1–20, normalized by the SD of CTRL over the years 1–20 (*Materials and Methods*).

differential land and ocean warming, reducing relative humidity over land (29), as highlighted in ATMO.

Physiological Effects Have a Critical Impact on the Variables of the Water Cycle. Field experiments (12, 15, 20) and observations (30) have shown that higher [CO_2] can stimulate plant growth within an observed range of nearly zero up to ~12% at a doubling of [CO_2] depending on species, climates, nutrient availability, and other stresses. Land-surface models capture a similar range (31). We find that the leaf area index (LAI) indeed increases almost everywhere except in Amazonia and central Africa (*SI Appendix,* Fig. S6*A*), where LAI is already high and further growth is thus limited (12). The physiological effect (*SI Appendix,* Fig. S6*C*) is, as expected, the primary driver of LAI changes over 89% of land

accounting for two-thirds of the change globally (*SI Appendix,* Figs. S6*D* and S7*A*). Exceptions are the northern latitudes where radiative effects (*SI Appendix,* Fig. S6*D*) induce warmer temperatures and a longer growing season (31) (*SI Appendix,* Fig. S6*B*), and the Amazon basin, where the combined negative contributions of the precipitation decline (Fig. 1*B* and *SI Appendix,* Fig. S6*D*) and the radiatively induced R_n increase (Fig. 1*E* and *SI Appendix,* Fig. S6*D*), cancel out the physiological effects (*SI Appendix,* Fig. S6 *C* and *D*).

Changes in ET under elevated [CO_2] vary widely across the globe (Fig. 2*A*) and are mostly controlled by physiological effects, which account for 58% of the changes globally (Fig. 3*A* and *SI Appendix,* Fig. S4*C*). In the energy-limited northern latitudes, higher ET is however mostly due to radiative effects and
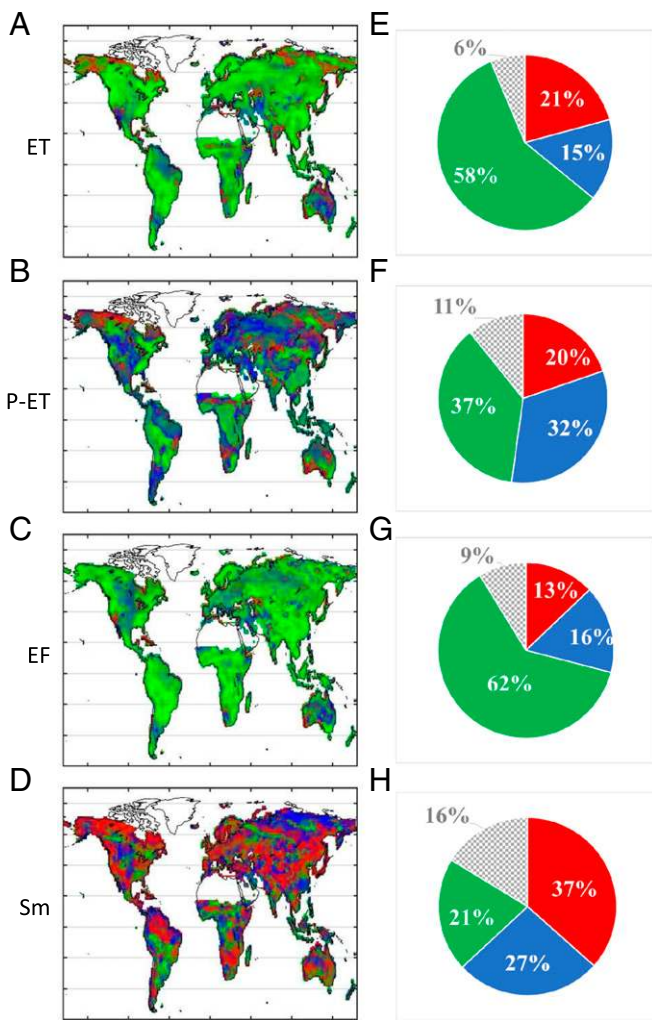
Fig. 3. Decomposition along the three main drivers of ET (*A*), P-ET (*B*), EF (*C*), and Sm (*D*) in CTRL. Green quantifies the effect of the vegetation physiology based on the run PHYS; red and blue quantify the contribution of, respectively, net radiation and precipitation, based on a multiple linear regression of ATMO. Pie charts show for ET (*E*), P-ET (*F*), EF (*G*), and Sm (*H*) the global average of each contribution, weighted by the total effect including error terms, reported as a gray shaded area.

accompanying increased precipitation (Figs. 2*B* and 3*A* and *SI Appendix,* Fig. S4*A*). Tropical rainforests, which are also energy-limited, display an increase in ET from radiative effects (Fig. 2*B*) but this effect is overcompensated by the physiological response of stomata to [CO_2] (Fig. 2*C*). The Mediterranean, Central America, and West Africa all exhibit reduced ET (Fig. 2*A*) in response to radiatively driven precipitation declines (Fig. 2*B*), but are also largely physiologically controlled (Fig. 3*A* and *SI Appendix,* Figs. S4 *A–C* and S7*B*).

The response of P-ET, i.e., long-term runoff (Fig. 2*D*), reflects the changes in both P and ET, and should be more strongly related to radiative changes as they mostly alter precipitation. Nonetheless, physiology still slightly dominates precipitation changes of P-ET, 37% vs. 32% of the total changes, respectively (Fig. 3*B*). In CTRL, the response is a smoothed version of the precipitation response (Fig. 1*A*) and does not reflect the increase in E_p (Fig. 3*B*) (6), further confirming that E_p is not a pertinent variable of changes in ET in the future (6). The geographical structure of P-ET thus largely reflects global warming changes (Fig. 2*E*). Physiological effects and their impact on ET (Fig. 2*C*) drive the P-ET response in the regions where ET changes are the

largest (Eastern United States,, central South America, Southeast Asia, and central Africa) (*SI Appendix,* Fig. S9*I*); they contribute most to P-ET in about one-third of the globe (Fig. 3*B* and *SI Appendix,* Fig. S4*F*). Precipitation accounts for about one-third of the P-ET changes (Fig. 3*B* and *SI Appendix,* Fig. S4*E*) and dominates the P-ET response in one-quarter of the globe (*SI Appendix,* Fig. S7*C*), which is a much larger fraction than for other stress indices such as LAI, ET, EF, or soil moisture. Over Western Europe, the northern part of Amazon, and southern South America, the decreasing trend in precipitation (Fig. 1*A*) has a large impact on P-ET. Radiation and related temperature increase drives P-ET change in the northern latitudes and in some semiarid regions (Fig. 3*B* and *SI Appendix,* Fig. S4*D*). However, one-third of the globe surface is not dominated by one single factor, and only their combined effects can explain the overall response (*SI Appendix,* Fig. S7*C*). This multimodel analysis of P-ET shows that both total greenhouse gas effects (as assessed in ATMO) and PHYS play a very significant role in long-term runoff similarly to a previous single Earth system model analysis (19).

The EF (latent heat flux divided by the total energy input) and its associated quantity, the Bowen ratio (sensible heat flux divided by latent heat flux), measure the surface energy partitioning toward ET and its impact on the overlying atmosphere (32, 33), and reflects ecosystem stress. While changes in EF are constrained by ET, they are impacted by the energy cycle changes as well. Both the radiative flux and EF changes impact the global changes in evaporation and precipitation (1). Since ET equals EF times the radiative flux, the responses of ET and EF are related but distinct, especially in regions where radiative changes are large, such as in cold regions. The linear combination of radiative and physiological effects very well explains the spatial patterns of EF in CTRL (Fig. 2*G*). Radiative (Fig. 2*H* and *SI Appendix,* Fig. S7*D*) and physiological effects (Fig. 2*I* and *SI Appendix,* Fig. S7*D*) show strong and opposite control on EF. Radiative effects increase EF (34), except in the Mediterranean, Central America, West Africa, and around the Amazon delta (Figs. 2*H* and 3*C* and *SI Appendix,* Figs. S4*G* and S7*D*). On the contrary, physiological effects have a large negative impact on EF (Fig. 2*I* and *SI Appendix,* Fig. S7*D*) in most regions (79% of the globe, *SI Appendix,* Fig. S7*D*) and especially in tropical regions (Fig. 3*C* and *SI Appendix,* Fig. S4*I*), as decreases in transpiration due to stomatal closure under rising [CO_2] are not compensated by saved soil moisture resources (17, 35) or increased LAI, which is already very high in tropical regions. In Alaska, Siberia, Australia, and the horn of Africa, the physiological-induced decrease of EF indicates increased partitioning toward sensible heating compared with ET and thus increased temperature through land–atmosphere feedback (36). It is therefore critical to correctly represent physiological effects in models to estimate future land–atmosphere interactions and extremes (17). Precipitation (Fig. 3*C* and *SI Appendix,* Fig. S4*H*) is a major driver of EF changes in Europe, Australia, in the Great Plains, and some of Central and South America. In the northern west coast of South America, EF decreases significantly, while ET tends to increase because of increased radiative effect (Fig. 2 *A*, *B*, and *G*). In Northern latitudes regions like Québec or central northern Russia, EF increases slightly but ET increases much more because of the additional radiative heating (Fig. 2 *A*, *B*, and *G*). Overall though, physiology accounts for the majority (almost two-thirds) of the EF changes (Fig. 3*C* and *SI Appendix,* Fig. S4*I*).

Growing season soil moisture at 2-m depth (SM_{2m}) (*Materials and Methods*) changes almost everywhere but the sign and magnitude of the response varies widely across the globe (Fig. 2*J*). SM_{2m} is influenced by changes in seasonality imposed by changes in phenology and LAI (*SI Appendix,* Fig. S6*C*) (17, 37). Most of the soil moisture decrease (Fig. 2*J*) is due to radiative effects (Figs. 2*K* and 3*D* and *SI Appendix,* Fig. S4*J*), whereas physiological effects tend to increase SM_{2m} (Fig. 2*L*), especially in equatorial Africa, South America, South Asia, and Indonesia (Fig. 2*J*). Soil moisture does not homogeneously change over the whole soil column, consistent with recent findings (38). Soil moisture changes are often thought to be driven by changes in P,

but this is confirmed only over a very small fraction of the globe (Fig. 3*D* and *SI Appendix*, Figs. S4*K* and S7*E*), and, overall, soil moisture changes have no unique global driver. Large fractions of the globe are impacted by radiative changes, including the Amazon and most of western Europe (Fig. 3*D* and *SI Appendix*, Fig. S4*J*), where precipitation also declines (Fig. 1*A*). Vegetation and land–atmosphere interactions are the main drivers of soil moisture changes in regions including South America, eastern United States, Southeast Asia, and some places in central Africa (*SI Appendix*, Fig. S9*O*). In addition, soil moisture variations are strongly nonlinear so that a linear decomposition does not explain all of the features observed (*SI Appendix*, Figs. S1–S3 and S6*E*), emphasizing that predicting soil moisture is more complicated than other stress indices.

Discussion

The control of precipitation on the future terrestrial water cycle is weak in general and represents the dominant control for only a small fraction of the Earth, consistent with recent remote sensing observations showing stronger vegetation response to atmospheric aridity compared with precipitation (39). In particular, precipitation trends are only a minor factor for biomass growth (as measured by LAI, *SI Appendix*, Fig. S6 *A*–*C*) and energy partitioning (as indicated by EF, Fig. 2 *G*–*I*). We note that the response over the Amazon basin is heavily influenced by net radiation changes rather than by physiological or precipitation effects (Fig. 3). In energy-limited ecosystems such as the Amazon, changes in radiation will become one of the primary drivers of transpiration and ecosystem functioning (40). Our conclusions are not strongly affected by additional land-use and land-cover changes or the addition of aerosols, as present in the RCP 8.5 simulations, which overall behave similarly to the simplified 1% yearly increase CO_2 experiments (*SI Appendix*, Fig. S1). Soil moisture appears to be the most complex and nonlinear variable and is also affected by uncertain land-use and land-cover change and vegetation response (41). Our study illustrates how deeply the physiological effects due to increasing atmospheric $[CO_2]$ impact the continental water cycle. Contrary to previous wisdom, changes in precipitation and radiation do not play the primary role in future drying and moistening in most regions. Rather, biosphere physiological effects and related biosphere–atmosphere interactions (42) are key for predicting future continental water stress as represented by ET, long-term runoff, EF, or leaf area index. In turn, vegetation water stress largely regulates land carbon uptake (43), further emphasizing how tightly the future carbon and water cycles are coupled so that they cannot be evaluated in isolation.

Materials and Methods

We used outputs from six Earth system models (ESM) from the idealized single-forcing CMIP5 (25) experiments with $[CO_2]$ increasing either in the atmospheric model only, in the vegetation model only, or in both, at a rate of 1% per year. The combined vegetation and atmospheric model $[CO_2]$ increase is called CTRL (1pctCO2 in CMIP5 terminology). We call PHYS the vegetation model $[CO_2]$ increase with no atmospheric model increase (esmFixClim1 in the CMIP5 terminology). We call ATMO the converse simulations, with atmospheric and no vegetation $[CO_2]$ increase (esmFdbk1 in CMIP5 terminology). The three runs are replicas of the same experiment, in which the $[CO_2]$ is increased for 140 y by 1% each year starting from preindustrial $[CO_2]$ levels in 1850 (except for HadGEM2-ES which starts in 1860).

The data are available for six models: bcc-csm1-1, CanESM2, CESM1-BGC, GFDL-ESM2M, HadGEM2-ES, and NorESM1-ME. For most of the models only one ensemble member is available for those experiments (r1i1p1 in the CMIP5 terminology), so we consider only one ensemble member per model.

The sum of ATMO and PHYS is very close to CTRL (*SI Appendix*, Figs. S2 and S3), indicating that the runs are indeed independent, and justifies this linear decomposition. In particular, for example, rare and extreme events caused by increased warming do not significantly impact PHYS effects on the future mean state in these simulations. Soil moisture, which shows more nonlinearities, is an exception. We also emphasize that because of slight differences in each ensemble member initial condition, one should not expect to obtain a perfect match between the combined ATMO + PHYS and CTRL. In

particular, regional variations should be expected and due to the internal climate variability.

These idealized runs differ from the more typical CMIP5 Representative Concentration Pathways 8.5, an emission scenario from 2005 to 2100 that includes prescribed changes in land-use and land-cover scenarios, as well as aerosol and ozone forcing. Also, the $[CO_2]$ increase is different between RCP 8.5 (ending at 936 ppm in 2100) and the 1% per year runs (ending at 1,145 ppm after 140 y of simulation). For comparison with the idealized 1% runs, we combined RCP 8.5 with the data from historical runs simulating the period 1850–2005 (historical in CMIP5 terminology). The resulting data for 1850–2100 are shown in *SI Appendix*, Figs. S1–S3, and are comparable in terms of geographical features to the 1% simulations.

Our analysis is based on monthly averaged outputs. We consider one value of a given water stress indicator for each year, and suggest the use of the most relevant period of the year for each variable and localization. It makes more sense to use annual average for precipitation and ET, and P-ET to obtain the total water fluxes—as ET is very small in cold winter regions. We also use the annual average for the net radiation and LAI. However, summer is the dominant growing season whether in tropics, midlatitudes, or high latitudes, but not around the equator, and so plant soil moisture stress is more present and relevant in summer than at other times of year. Hence, we use the summertime mean (i.e., June, July, and August for latitudes between [10; 90] and December, January, and February for latitudes between [−90; −15]) for EF, VPD, and soil moisture, three variables that indicate a stress, except around the equator (latitudes between [−15; 10]) where, in the Congo for instance, there are two dry/wet seasons. Around the equator, selecting only one season would thus lead to a subjective assessment of dryness, as there is minimal dryness in the wet seasons, and ultimately the annual signal is dominated by the dry seasons. The [−15; 10] latitude range was chosen so that the transition with the local summer averaging zones looks smooth, and so that the equatorial range stays as small as possible.

We regrid each model to a common 1° × 1° grid to later compute the intermodel average. The change of a variable X is normalized before the intermodel averaging by the interannual variability and is calculated according to the following formula: $\Delta X = \overline{X_{fut}} - \overline{X_{hist}}/\sigma(X_{hist})_{CTRL}$, where $\overline{X_{fut}}$ is the mean of X over years 89–118 of the runs CTRL, PHYS and ATMO (respectively, 2070–2099 for RCP 8.5), $\overline{X_{hist}}$ is the mean of X over years 1–20 (respectively, 1939–1968), and $\sigma(X_{hist})_{CTRL}$ is the SD of X over the same period of the run CTRL. We have chosen the averaging periods so that the mean CO_2 concentrations in all four sets of runs are similar (*SI Appendix*, Table S1). We then compute the standardized change ΔX intermodel average. For comparison, *SI Appendix*, Figs. S8 and S9 show for all of the variables presented in Figs. 1 and 2 the change in ATMO and PHYS relative to CTRL: $RUN/CTRL = [\overline{X_{fut}} - \overline{X_{hist}}]_{RUN}/[\overline{X_{fut}} - \overline{X_{hist}}]_{CTRL}$.

Net radiation is computed using the net downward minus upward longwave and shortwave radiation fluxes. EF is defined as the monthly ratio of the latent heat flux to the sum of the latent and the sensible heat fluxes. VPD is computed from the relative humidity and the saturation vapor pressure, calculated from the monthly averaged temperature. Soil moisture at 2 m and at 30 cm are interpolated using the model soil moisture profiles. As the number of layers varies across models, we first linearly interpolate the profiles of each model and each annual data point (e.g., after the seasonal averaging), extract the value at 2-m depth and 30-cm depth, and then apply the same routine as for the other variables.

SI Appendix, Fig. S11 shows the number of models that agree with the sign of the ΔX intermodel average. Only the soil moisture intermodel average change shows wide areas of mismatch with individual model change sign.

We decompose changes in each water stress variable X (P-ET, LAI, etc.) into three terms (Fig. 3 and *SI Appendix*, Fig. S4): the change due to the effect of R_n, the change due to the effect of P, and the change due to the effect of the physiology. Changes due to R_n are not differentiated from correlated changes in air temperature and VPD, as they are too collinear to yield unique linear decomposition.

This translates into the following equation [1] decomposing changes in water cycle variables, due to R_n and precipitation changes in ATMO and physiological changes in PHYS (and related changes in atmospheric VPD and R_n through land–atmosphere interactions, as seen in Figs. 1 and 2):

$$\Delta X = \left\{ \left[\frac{\partial X}{\partial Rn} \cdot \Delta Rn\right]_{ATMO} + \left[\frac{\partial X}{\partial P} \cdot \Delta P\right]_{ATMO} + [Decomposition\ error]_{ATMO} \right\}$$
$$+ [\Delta X]_{PHYS} + [Decomposition\ error\ into\ ATMO\ \&\ PHYS]. \quad [1]$$

First we regrid X to 1 × 1° and temporally (annually except for the soil moisture at 2 m) average it as for Fig. 2. Then we apply a multiple linear

regression of the variable X of ATMO with respect to the drivers P or R_n, over the 140 y of the six models data of X. Hence we regress against 140 × 6 values for each grid point and each variable X, P, R_n. Those decomposed PHYS and ATMO runs help us uniquely define the sensitivity. This contrasts with CTRL where all variables are evolving jointly in response to both surface physiological and radiative changes so that a uniquely defined decomposition is nearly impossible. The decomposition error terms are reported in *SI Appendix*, Figs. S2 and S3; the fraction of variance explained by the multiple linear regression (R^2) is in coherence with the fact that LAI and EF are dominated by physiological effects (Fig. 3*C* and *SI Appendix*, Fig. S6*D*), but large for P-ET (*SI Appendix*, Fig. S10).

A linear regression on net radiation and precipitation cannot account for all of the variance explained, as we did not include other modified variables such as temperature, relative humidity, or wind. However, given the very strong correlation (nearly 1) of temperature with net radiation, a unique linear decomposition cannot be found. The other terms (relative humidity, wind, and nonlinearities), as well as nonlinearities and ensemble variations, explain the nonunity R^2 (*SI Appendix*, Fig. S10). However, in most regions R^2 is very high, emphasizing that precipitation and net radiation (and related temperature changes) are the primary drivers of the change. In the CO_2 physiological runs, precipitation changes as well as mean temperature changes are small (Fig. 1), so that it is fair to ignore precipitation influence on the changes due to physiological effects.

It should also be noted that PHYS and ATMO are strictly independent and cannot have cross-correlation. The decomposition of CTRL into ATMO and PHYS is not perfect but works well, as shown in *SI Appendix*, Figs. S2 and S3. The effect of the linearization in ref. 1 in the independent PHYS and ATMO runs is further compared with the full nonlinear response of the CTRL runs in *SI Appendix*, Figs. S2 and S3. ATMO and PHYS contribute quite independently and linearly to CTRL (*SI Appendix*, Figs. S2 and S3). However, if we use the decomposition of ATMO changes along the precipitation and the net radiation (as in Fig. 3 and *SI Appendix*, Fig. S4) to reconstruct an equivalent to CTRL, the result is satisfactory except for EF at northern latitudes and in eastern Africa (*SI Appendix*, Figs. S2 and S3), and especially for the soil moisture (*SI Appendix*, Figs. S2 and S3), indicating nonlinearities, consistent with an overall low R^2 (*SI Appendix*, Fig. S10). This further emphasizes the difficulty to predict the change in soil moisture.

We end up with a triplet (R, G, B) with R, G, and B in [0; 1] for each pixel defined as the absolute normalized sensitivity to net radiation, physiology, and precipitation changes, respectively:

$$R = \frac{\left|\left[\frac{\partial X}{\partial Rn}.\Delta Rn\right]_{ATMO}\right|}{\left|\left[\frac{\partial X}{\partial Rn}.\Delta Rn\right]_{ATMO}\right| + \left|\left[\frac{\partial X}{\partial P}.\Delta P\right]_{ATMO}\right| + \left|[\Delta X]_{PHYS}\right|},\quad [2]$$

$$G = \frac{\left|[\Delta X]_{PHYS}\right|}{\left|\left[\frac{\partial X}{\partial Rn}.\Delta Rn\right]_{ATMO}\right| + \left|\left[\frac{\partial X}{\partial P}.\Delta P\right]_{ATMO}\right| + \left|[\Delta X]_{PHYS}\right|},\quad [3]$$

$$B = \frac{\left|\left[\frac{\partial X}{\partial P}.\Delta P\right]_{ATMO}\right|}{\left|\left[\frac{\partial X}{\partial Rn}.\Delta Rn\right]_{ATMO}\right| + \left|\left[\frac{\partial X}{\partial P}.\Delta P\right]_{ATMO}\right| + \left|[\Delta X]_{PHYS}\right|}.\quad [4]$$

The triplet (R, G, B) is used to color the pixel with the combination of (red, green, blue) in Fig. 3, as an indicator of absolute net radiation, physiology, and precipitation changes. On all plots we discard pixels where LAI is below 0.2. Fig. 3 reports also pie charts of global averages of R, G, and B values, weighted by the total effect including error terms, reported in these pie charts as a dashed gray area.

1. Held IM, Soden BJ (2006) Robust responses of the hydrological cycle to global warming. *J Clim* 19:5686–5699.
2. Seager R, et al. (2014) Causes of increasing aridification of the mediterranean region in response to rising greenhouse gases. *J Clim* 27:4655–4676.
3. Penman HL (1948) Natural evaporation from open water, bare soil and grass. *Proc R Soc A* 193:120–145.
4. Durack PJ, Wijffels SE, Matear RJ (2012) Ocean salinities reveal strong global water cycle intensification during 1950 to 2000. *Science* 336:455–458.
5. Greve P, Seneviratne SI (2015) Assessment of future changes in water availability and aridity. *Geophys Res Lett* 42:5493–5499.
6. Swann ALS, Hoffman FM, Koven CD, Randerson JT (2016) Plant responses to increasing CO2 reduce estimates of climate impacts on drought severity. *Proc Natl Acad Sci USA* 113:10019–10024.
7. Milly PCD, Dunne KA (2016) Potential evapotranspiration and continental drying. *Nat Clim Chang* 6:946–949.
8. Byrne MP, O'Gorman PA (2015) The response of precipitation minus evapotranspiration to climate warming : Why the "'wet-get-wetter, dry-get-drier'" scaling does not hold over land *. *J Clim* 28:8078–8092.
9. He J, Soden BJ (2016) A re-examination of the projected subtropical precipitation decline. *Nat Clim Chang* 7:53–57.
10. Scheff J, Frierson DMW (2014) Scaling potential evapotranspiration with greenhouse warming. *J Clim* 27:1539–1558.
11. Good SP, Noone D, Bowen G (2015) Hydrologic connectivity constrains partitioning of global terrestrial water fluxes. *Science* 349:175–177.
12. Norby RJ, Zak DR (2011) Ecological lessons from free-air CO2 enrichment (FACE) experiments. *Annu Rev Ecol Evol Syst* 42:181–203.
13. de Boer HJ, et al. (2011) Climate forcing due to optimization of maximal leaf conductance in subtropical vegetation under rising CO2. *Proc Natl Acad Sci USA* 108:4041–4046.
14. Lammertsma EI, et al. (2011) Global CO2 rise leads to reduced maximum stomatal conductance in Florida vegetation. *Proc Natl Acad Sci USA* 108:4035–4040.
15. Ainsworth EA, Long SP (2005) What have we learned from 15 years of free-air CO2 enrichment (FACE)? A meta-analytic review of the responses of photosynthesis, canopy properties and plant production to rising CO2. *New Phytol* 165:351–371.
16. Warren JM, et al. (2011) Ecohydrologic impact of reduced stomatal conductance in forests exposed to elevated CO2. *Ecohydrology* 4:196–210.
17. Lemordant L, Gentine P, Stéfanon M, Drobinski P, Fatichi S (2016) Modification of land-atmosphere interactions by CO2 effects: Implications for summer dryness and heatwave amplitude. *Geophys Res Lett* 43:10240–10248.
18. Leuzinger S, Körner C (2007) Water savings in mature deciduous forest trees under elevated CO2. *Glob Change Biol* 13:2498–2508.
19. Betts RA, et al. (2007) Projected increase in continental runoff due to plant responses to increasing carbon dioxide. *Nature* 448:1037–1041.
20. Mccarthy HR, et al. (2007) Temporal dynamics and spatial variability in the enhancement of canopy leaf area under elevated atmospheric CO2. *Glob Change Biol* 13:2479–2497.
21. Sellers PJ, et al. (1996) Comparison of radiative and physiological effects of doubled atmospheric CO_2 on climate. *Science* 271:1402–1406.
22. Berg A, et al. (2016) Land–atmosphere feedbacks amplify aridity increase over land under global warming. *Nat Clim Chang* 6:869–874.
23. Scheff J, Frierson DMW (2015) Terrestrial aridity and its response to greenhouse warming across CMIP5 climate models. *J Clim* 28:5583–5600.
24. Greve P, et al. (2014) Global assessment of trends in wetting and drying over land. *Nat Geosci* 7:716–721.
25. Taylor KE, Stouffer RJ (2011) Meehl G a (2007) a summary of the CMIP5 experiment design. *WORLD* 4:1–33.
26. Kapnick SB, Delworth TL (2013) Controls of global snow under a changed climate. *J Clim* 26:5537–5562.
27. Krasting JP, Broccoli AJ, Dixon KW, Lanzante JR (2013) Future changes in northern hemisphere snowfall. *J Clim* 26:7813–7828.
28. Gentine P, et al. (2013) A probabilistic bulk model of coupled mixed layer and convection. Part II: Shallow convection case. *J Atmos Sci* 70:1557–1576.
29. Byrne MP, O'Gorman PA (2016) Understanding decreases in land relative humidity with global warming : Conceptual model and GCM simulations. *J Clim* 29:9045–9061.
30. Campbell JE, et al. (2017) Large historical growth in global terrestrial gross primary production. *Nature* 544:84–87.
31. Zhu Z, et al. (2016) Greening of the earth and its drivers. *Nat Clim Chang* 6:791–795.
32. Gentine P, Entekhabi D, Chehbouni A, Boulet G, Duchemin B (2007) Analysis of evaporative fraction diurnal behaviour. *Agric Meteorol* 143:13–29.
33. Gentine P, Entekhabi D, Polcher J (2011) The diurnal behavior of evaporative fraction in the soil–vegetation–atmospheric boundary layer Continuum. *J Hydrometeorol* 12:1530–1546.
34. Hartmann DL (1994) *Global Physical Climatology* (Academic Press, San Diego), pp 140–147.
35. Gray SB, et al. (2016) Intensifying drought eliminates the expected benefits of elevated carbon dioxide for soybean. *Nat Plants* 2:16132.
36. Seneviratne SI, et al. (2010) Investigating soil moisture-climate interactions in a changing climate: A review. *Earth Sci Rev* 99:125–161.
37. Boisier JP, Ciais P, Ducharne A, Guimberteau M (2015) Projected strengthening of Amazonian dry season by constrained climate model simulations. *Nat Clim Chang* 5:656–660.
38. Berg A, Sheffield J, Milly PCD (2017) Divergent surface and total soil moisture projections under global warming. *Geophys Res Lett* 44:236–244.
39. Konings AG, Williams AP, Gentine P (2017) Sensitivity of grassland productivity to aridity controlled by stomatal and xylem regulation. *Nat Geosci* 10:284–288.
40. Pieruschka R, Huber G, Berry JA (2010) Control of transpiration by radiation. *Proc Natl Acad Sci USA* 107:13372–13377.
41. Alkama R, Cescatti A (2016) Biophysical climate impacts of recent changes in global forest cover. *Science* 351:600–604.
42. Green JK, et al. (2017) Regionally strong feedbacks between the atmosphere and terrestrial biosphere. *Nat Geosci* 10:410–414.
43. Poulter B, et al. (2014) Contribution of semi-arid ecosystems to interannual variability of the global carbon cycle. *Nature* 509:600–603.

Lemordant et al.